

RF-SQUID prepared on MgB₂ variable-thickness bridge by AFM scratching

M. Gregor, T. Plecenik, M. Prašćák, R. Mičunek, M. Kubinec, V. Gašparík, M. Grajcar, P. Kúš and A. Plecenik.

Department of Experimental Physics, Comenius University, SK-84248 Bratislava, Slovakia

(Dated: April 21, 2019)

We present the preparation of radio-frequency superconducting quantum interface devices (SQUID) on MgB₂ thin film with $T_c \approx 32$ K. Variable-thickness bridge was prepared by combination of optical lithography and AFM scratching technique. The critical current of nanobridge was $0.35 \mu\text{A}$ at 4.2 K. Non-contact measurements of current-phase characteristics and critical current vs. temperature have been investigated on our SQUID structures.

PACS numbers: 74.72.-h, 85.25.Dq, 74.50.+r, 85.25.Cp, 74.76.Db

Since the discovery of superconducting properties of MgB₂,¹ many techniques to prepare of weak links has been made worldwide. The relative high critical temperature of MgB₂, metallic character, good stability and low anisotropy make MgB₂ interesting for use in weak links or superconducting quantum interface devices. To measure the energy gap a number of tunneling experiments with normal contacts have been performed.² Apart from tunnel junction, weak links with non-tunnel-type conductivity have been attracting increasing attention, such as point contact, Dayem type bridge, constant and variable thickness bridge. A main advantage of non-tunnel-type junction is its low capacitance. Nanobridges with dimensions L_{eff} sufficiently small relative to coherence length ξ have nearly ideal Josephson behavior. Reported value of coherence length is 5.2 nm.³ Importantly, also wider bridge can show a significant current-phase relationship, proved the width of the bridge is comparable to, or smaller than the effective London penetration depth λ_{eff} . Reported values for the bulk penetration depth λ for MgB₂ vary from 140 to 180 nm.⁴ Zhang et al.⁵ reported an MgB₂ SQUID based on point contact at 19 K. Burnell et al.⁶ realized by localized ion damage in MgB₂ film SQUID operated up to 20 K. Several groups prepared SQUID using focused ion beam and produced nanobridges with dimensions smaller than effective London penetration depth λ_{eff} .⁴ Burnell et al.⁷ reported MgB₂ SQUID prepared by FIB operated from 10 K to 24 K, with magnetic flux noise at 20 K low as $14 \mu\Phi_0\text{Hz}/\sqrt{Hz}$. Lithography using Atomic Force Microscope has been came up powerful technology, which allows to create structures with a nanometer scale resolution suitable for cryogenic application. Atomic force microscope can pattern surface in different ways - local oxidation or scratching. Some researchers published technology of local electrochemical oxidation of the surface of Nb and NbN thin films by voltage biased tip⁸ and produced Dayem and variable thickness nanobridges. Another produced nanostructures using tip-surface mechanical interaction leading to surface plowing or scratching⁹ and produced typical Dayem-type bridge in a Al film with dimension $100 \times 100 \text{ nm}^2$. We focus our attention on preparation of RF-SQUID variable-thickness bridge on MgB₂ superconductor by AFM scratching through the photoresist. The main advantage of our approach

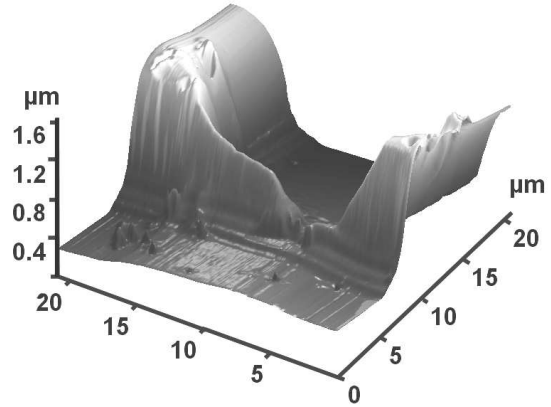


FIG. 1: AFM scan of the MgB₂ variable thickness bridge prepared on 200 nm MgB₂ thin film with 1.5 μm thick photoresist.

is possibility to prepare nanostructures on the hard materials through the resist without ion damage, which is produced in focused ion beam machining. By the post-etching with low energy Ar ions we are able to change continuously dimensions of bridge.

Superconducting MgB₂ thin films were prepared by magnetron sputtering on the sapphire substrate and ex-situ annealing in vacuum chamber. Deposition process was realized by two independent magnetrons. Technology of MgB₂ thin film preparation was described in Ref. 10. Atomic Force Microscope has been used for surface roughness analysis of thin films, for preparing of weak links and for investigating of weak links. Scanning has been done in semi-contact mode using standard Si tip with W₂C coating or diamond like coating. The maximum lateral scan range of piezo tube is $50 \times 50 \mu\text{m}^2$, the maximum vertical range is 2 μm . Typical curvature radius of tip is 30 nm and resonant frequency is about 255 kHz. The spring constant of the cantilevers used is 20-30 N/m. On these smooth MgB₂ surfaces we prepared RF-SQUID with microstrip by optical lithography (3 μm wide strip). We used positive photoresist for direct optical lithography and argon ion etching with energy of ions 650 eV and ion current 50 mA for determination of the microstructure. After formation of structures by Ar ion

etching, the resist was not removed from MgB₂ strip and on such strip with photoresist coating, AFM scratching was applied. Our SQUID consists of washer (50 × 50 μm inner and 2000 × 2000 μm outer dimension) for better concentration of magnetic flux and 10 μm wide slit.

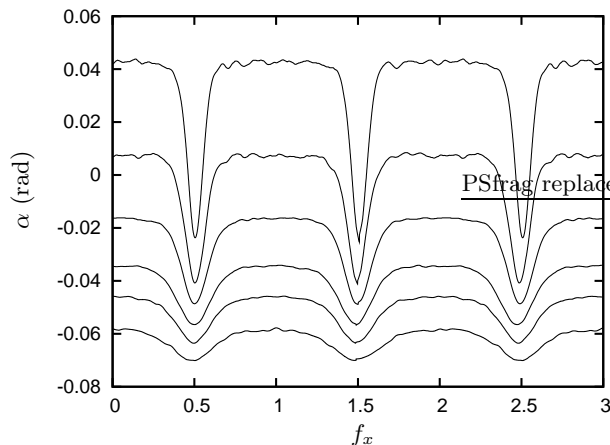


FIG. 2: Phase shift between voltage across the tank and driving current measured at various temperature as a function of normalized external magnetic flux $f_x = \Phi_x/\Phi_0$. From top to bottom, the data correspond to $T=4.2, 6.4, 7.8, 9, 10.4,$ and 12.6 K

Micro-strip with 10 μm length and 3 μm width is close to inner hole, into which variable-thickness bridge was prepared with AFM scratching. For AFM scratching (nanolithography) it is necessary to know setpoint of cantilever deflection. When the cantilever is approached to surface sample in contact mode, cantilever is deflected by known force, called deflection force. For simple imaging the deflection force is kept constant using the feedback loop. Scratching is achieved by increasing deflection of cantilever, i.e. by increasing the setpoint several times. The width and the depth of the grooves depend on the deflection force. By scratching of resist across the strips we produced small variable-thickness bridge with submicrometer dimension. We applied additional Ar ion beam etching and gradually removed MgB₂ from the strip, so that we achieved the final thickness of the MgB₂ strip after the etching about few nm and width about 100 nm. Figure 1 shows variable-thickness bridge before removing of photoresist. The investigated SQUID is placed close to a parallel LC tank circuit. This resonant detection system consists of a solenoid copper coil ($L_T \approx 73$ nH) and small capacitance ($C_T \approx 700$ pF). Tank circuit is fed from current source at the resonant frequency 24 MHz, which produces alternating flux in the SQUID of amplitude $MQI_b \sin \omega_0 t$, where $Q = 80$ is the quality factor of our tank circuit, $M \approx 0.12$ nH is mutual inductance and $I_b \sin \omega_0 t$ is the bias current. The DC flux in the SQUID is produced by the same copper coil. The signal from the tank circuit is amplified by the first stage of our amplifier located close to the tank circuit at liquid helium temperature. The cryogenic amplifier consists of

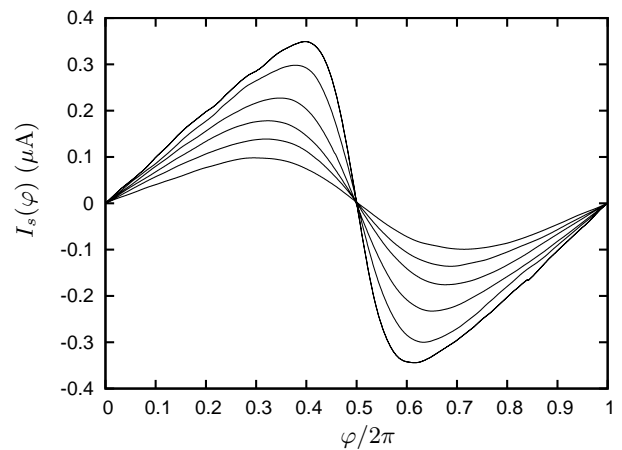


FIG. 3: $I_s(\varphi)$ characteristics calculated from phase characteristics (see Fig. 2). The curves corresponds to temperature, from top to bottom, $T=4.2, 6.4, 7.8, 9, 10.4,$ and 12.6 K.

high electron mobility field effect transistor promoting low noise figure (0.4dB), high gain (18dB) and wide dynamic range. This amplifier stage provides impedance matching to 50 Ω coaxial cable and approximately 10dB gain. The output signal is further amplified by following stages at room temperature. The second stage is of similar design as the cryogenic stage and the last stage is a 30dB MMIC gain block. The overall gain is above 50dB with noise figure about 0.5dB at room temperature. The amplified signal is fed to a phase sensitive detector (Lock-in amplifier) from which the output is the amplitude and phase of the signal relating to the reference signal from the RF generator. Data acquisition and the measurement process is computer controlled via GPIB interface. The SQUID phase characteristics $\alpha(f_x)$ are shown in Fig.2. In order to obtain more information on microbridge superconducting weak link we have calculated its current-phase relationship (CPR) $I_s(\varphi) = I_c f(\varphi)$ using modified Rifkin-Deaver method^{11,12}. The resonance frequency of the tank circuit depends on the effective inductance defined as^{13,14}

$$L_{eff}(\varphi) = L \left(1 + \frac{1}{\beta f'(\varphi)} \right) \quad (1)$$

where L is inductance of the washer, $\varphi = 2\pi\Phi/\Phi_0$ is gauge-invariant phase difference across the Josephson junction, Φ is internal flux in the washer, Φ_0 is elementary magnetic flux quantum and $\beta = 2\pi LI_c/\Phi_0$ is normalized SQUID inductance. If $\beta < 1$, i.e. the SQUID is in nonhysteretic mode, we can determine the current-phase relationship from relation¹²

$$I_s(\varphi) = \frac{L_T(\Delta I)^2}{2\pi Q \Phi_0} \int_0^\varphi \tan \alpha(\phi) d\phi \quad (2)$$

where L_T is inductance of the tank coil, $\Delta I = 16.5 \mu A$ is a magnitude of the current in the coil producing magnetic flux Φ_0 in the rf squid, Q is quality factor of the

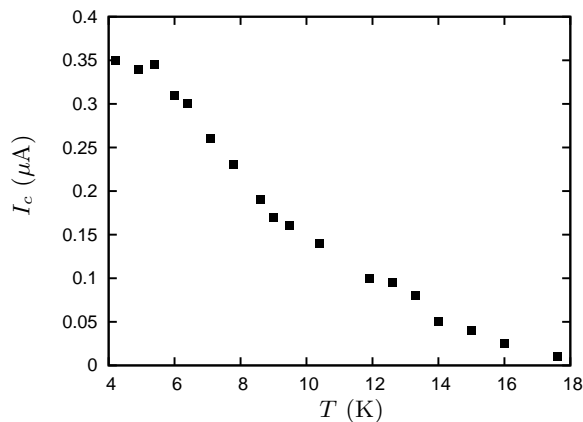


FIG. 4: Temperature dependence of the critical current of the weak link

tank circuit and $\phi = 2\pi\Phi_e/\Phi_0$ normalized external dc magnetic flux. The phase shift $\alpha(\phi)$ between voltage across the tank and driving current is measured experimentally. The calculated current-phase characteristics are shown in Fig. 3. The maximum of the $I_s(\varphi)$ characteristics is shifted towards $\varphi = \pi$. Such deviation from standard Josephson sinusoidal behavior was predicted by Kulik and Omelyanchuk^{15,16} for short Josephson junctions $d_{eff} \ll \xi$, where d_{eff} is effective length of the weak link.¹⁷ However, this condition can be hardly satisfied since $\xi \approx 5$ nm. Also temperature dependence (compare Fig. 4 with Fig. 9 in Ref. 17 or Fig. 14 in Ref. 12) indi-

cates that weak link is long with $d_{eff} > \xi$ and that critical temperature of the bridge T'_c is suppressed ($T'_c < T_c$). Thus, the shift of the maximum is caused by kinetic inductance of the junction, which can be characterized by parameter¹⁷

$$l = 2\pi \frac{\mathcal{L}I_c}{\Phi_0} \quad (3)$$

where \mathcal{L} is kinetic inductance of the weak links. If l is larger than unity the $I_s(\varphi)$ becomes multivalued and SQUID is in hysteretic regime even for $\beta < 1$. However, our SQUID is in nonhysteretic regime as one can expect for variable-thickness bridges.^{17,18} The thickness, width and length of the bridge in the thinnest region is estimated from the AFM picture (Fig. 1 to be 10, 200, and 100 nm, respectively).

To conclude our result show that AFM scratching through the soft material (our case - photoresist) is powerful technology, which can produce MgB₂ weak links with single valued Josephson current-phase relationship. Such weak links are promising for practical application and they can be incorporated into Josephson effect devices.¹⁹

Acknowledgments

This work was supported by grant VEGA 1/2011/05, APVT projects No. APVT-51-016604, APVT-20-011804 and project aAV/1126/2004.

¹ J. Nagamatsu, N. Nakagawa, T. Muranaka, Y. Zenitani, and J. Akimitsu, *Nature* **410**, 63 (2001).
² A. Plecenik, Š. Beňačka, P. Kúš, and M. Grajcar, *Physica C* **368**, 251 (2002).
³ D. K. Finnemore, J. E. Ostenson, S. L. Bud'ko, G. Laperot, and P. C. Canfield, *Phys. Rev. Lett.* **86**, 2420 (2001).
⁴ A. Brinkman, D. Veldhuis, D. Mijatovic, G. Rijnders, D. H. A. Blank, H. Hilgenkamp, and H. Rogalla, *Appl. Phys. Lett.* **79**, 2420 (2001).
⁵ Y. Zhang, D. Kinion, J. Chen, J. Clarke, D. G. Hinks, and G. W. Crabtree, *Appl. Phys. Lett.* **79**, 3995 (2001).
⁶ G. Burnell, D.-J. Kang, H. N. Lee, S. H. Moon, B. Oh, and M. G. Blamire, *Appl. Phys. Lett.* **79**, 3464 (2001).
⁷ G. Burnell, D. J. Kang, D. A. Ansell, H. N. Lee, S. H. Moon, E. J. Tarte, and M. G. Blamire, *Appl. Phys. Lett.* **81**, 102 (2002).
⁸ M. Fraucher, T. Fournier, B. Pannetier, C. Thirion, W. Wernsdorfer, J. Villegier, and V. Bouchiat, *Physica C* **368**, 211 (2002).
⁹ B. Irmer, R. H. Blick, F. Simmel, W. Gdel, H. Lorenz, and J. P. Kotthaus, *Appl. Phys. Lett.* **73**, 2051 (1998).

¹⁰ R. Mičunek, A. Plecenik, P. Kúš, M. Zahoran, M. Tomášek, M. v. T. Plecenik, M. Gregor, V. Jacko, M. K. J. Greguš, B. Grančič, and M. Mahel', *Physica C* **435**, 78 (2006).
¹¹ R. Rifkin and B. Deaver, *Phys. Rev. B* **13**, 3894 (1976).
¹² A. A. Golubov, M. Y. Kupriyanov, and E. Il'ichev, *Rev. Mod. Phys.* **76**, 411 (2004).
¹³ A. H. Silver and J. E. Zimmerman, *Phys. Rev.* **157**, 317 (1967).
¹⁴ A. Barone and G. Paterno, *Physics and Applications of the Josephson Effect* (JOHN WILEY & SONS, 1982).
¹⁵ I. O. Kulik and A. N. Omelyanchuk, *JETP Lett.* **21**, 96 (1975).
¹⁶ I. O. Kulik and A. N. Omelyanchuk, *Soc. J. Low. Temp. Phys.* **3**, 945 (1977).
¹⁷ K. K. Likharev, *Rev. Mod. Phys.* **51**, 101 (1979).
¹⁸ L. D. Jackel, W. H. Henkels, J. M. Warlaumont, and R. A. Buhrman, *Appl. Phys. Lett.* **29**, 214 (1976).
¹⁹ K. Likharev, *Dynamics of Josephson Junctions and Circuits* (Gordon and Breach Science Publishers, 1984).